Al-Azhar Bulletin of Science

Volume 34 | Issue 3 Article 6

2023
Section: Physics

Investigation of Role of Tungsten Ions on Structural and Optical Properties of Sodium Borosilicate Germanate Glass for Optoelectronic Applications

Mohamed Mundher
Physics department, Faculty of Science, Al-Azhar University, Cairo, Egypt

Mohammed A. Farag
Physics department, Faculty of Science, Al-Azhar University, Cairo, Egypt

Ayman A. Bendary
Physics department, Faculty of Science, Al-Azhar University, Cairo, Egypt

Mohamed Y. Hassaan
Physics department, Faculty of Science, Al-Azhar University, Cairo, Egypt, myhassaan@yahoo.com

Abu Bakr El-Bediwi
Physics Department, Faculty of Science, Mansoura University, Mansoura, Egypt

How to Cite This Article

Mundher, Mohamed; Farag, Mohammed A.; Bendary, Ayman A.; Hassaan, Mohamed Y.; and El-Bediwi, Abu Bakr (2023) "Investigation of Role of Tungsten Ions on Structural and Optical Properties of Sodium Borosilicate Germanate Glass for Optoelectronic Applications," *Al-Azhar Bulletin of Science*: Vol. 34: Iss. 3, Article 6.
DOI: https://doi.org/10.58675/2636-3305.1655

ORIGINAL ARTICLE

Investigation of Role of Tungsten Ions on Structural and Optical Properties of Sodium Borosilicate Germinate Glass for Optoelectronic Applications

Mohamed Mundher [a], Mohammed Abd El-Aity Farag [a], Ayman Abd El-Karim Bendary [a], Mohamed Yousry Hassaan [a,*], Abu Bakr El-Bediwi [b]

[a] Physics Department, Faculty of Science, Al-Azhar University, Cairo, Egypt
[b] Physics Department, Faculty of Science, Mansoura University, Mansoura, Egypt

Abstract

In the current work, the role of tungsten ions on the structural and optical properties of sodium borosilicate germinate glass with the composition [70 Na $_2B_4O_7$−15 SiO_2−(15-x) (Ge_2O_3) − x (WO_3) while, x = 0,2,4, 6, 8 mol %] were studied. Fast quenching method were used to prepare the glass samples. Experimental and empirical density results confirm the amorphous nature of the prepared samples. Fourier transform infrared, FTIR, results showed N_4 decreases as WO_3 increases. These results suggest that the decreasing in non-bridging oxygen (NBO), back conversion BO_4 to BO_3, occur by the increase of WO_3. Optical band gap show decreases from 3.3 down to 1.89 eV with increase in refractive index from 1.98 up to 2.35 these results indicate promising application for the prepared glasses in electric and optoelectronic applications.

Keywords: Optical properties, Borosilicate glass, Fourier transform infrared

1. Introduction

Glass is an amorphous, transparent, brittle and colourless material. Also, the structural properties of the glass can be improved by altering some components during the manufacturing process. Glass has versatile optical properties which is ideal for different optical applications. Depending on the purity and composition, glass can transmit light in both Infra-red and visible region of spectra. Borosilicate glasses have higher crystallization resistance compared with other glasses, which is useful in various technological applications [1]. Na^+ ion can break down the original network of boron by acting as charge compensator in the four coordinated boron [2−4]. Transition metal oxides in glass have different important applications [3−5]. While borate glasses have low melting point and high mechanical strength [6−11]. Bismuth ions in borate glasses have high density which nominate these glasses to be used as radiation shielding [12−14]. Tungsten oxide as a transition metal oxide has different valence states that play a important role in the electronic conduction. While Na^+ ions side by side with the BO_4 and nonbridging oxygens increase ionic conductions [15]. In this paper, the effect of tungsten ions on the optical absorption, density, infrared spectra, and optical energy of tungsten borosilicate germinate glass system was reported. The electrical properties of the obtained system, which is already published [15], along with the optical properties obtained in the current work, the prepared glass system could be very useful in many optical and optoelectronic application.

2. Experimental work

Glass samples with the composition [70 $Na_2B_4O_7$−15 SiO_2− (15-x) Ge_2O_3− (X) WO_3] where, x = 0, 2, 4, 6, and 8 mol. % were prepared by the

Received 5 September 2023; revised 12 September 2023; accepted 15 September 2023.
Available online 27 December 2023

* Corresponding author.
E-mail address: myhassaan@yahoo.com (M.Y. Hassaan).

https://doi.org/10.58675/2636-3305.1655

melt quenching technique. High purity of row oxides of $Na_2B_4O_7$, Ge_2O_3, SiO_2, and WO_3 were used. Samples were melted in porcelain crucible at 1200 °C for one hour. The molten was poured and quenched between two brass plates. Experimental density of the samples was measured by Archimedes's method using Toluene as an immersion liquid (FTIR) absorption spectra were obtained, by KBr method, in the wavenumber range of 400–2000 cm^{-1} using Bruker vertex80 v. The optical absorption and transmission spectra were measured at wavelengths between 200 and 1100 nm for the bulk glasses using Shimadzu 3600 UV–Vis spectrophotometer. The appearance of sample x = 0 is shown below.

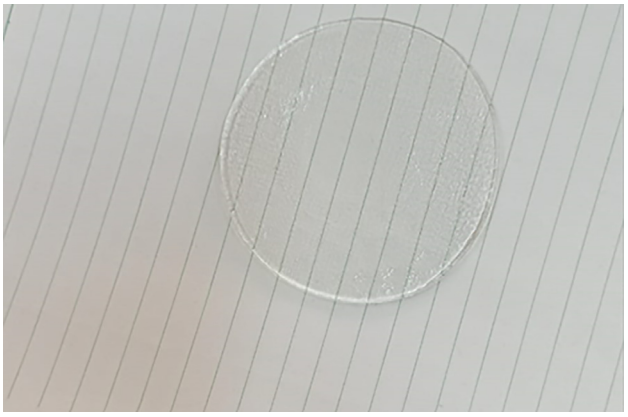

Appearance of sample X = 0.

3. Results and discussions

3.1. Density and molar volume

The density of the examined glasses was evaluated empirically using the liquid displacement method, and the results were compared to those found theoretically for the compositions' close-packed structures. For comparison, the experimental and empirical density values were both displayed in Fig. 1 as a function of WO_3 content. It is evident that both density values experimental and empirical grew steadily and linearly as WO_3 concentration increase for the compositions' close-packed structures. For comparison, the experimental and empirical density values were both displayed in Fig. 1 as a function of WO_3 content. It is evident that both density values experimental and empirical grew steadily and linearly as WO_3 concentration increase [16]. It is also noted that the empirical density is typically higher than the corresponding experimental density, as shown in Fig. 1 which confirm the short-range order in the samples under investigation. The difference between empirical and experimental density be explained as, the empirical density uses the crystalline density values of the glass component oxides while glass contains disorder with increase the overall volume which decrease the density of the glass than the empirical values. The behaviour of the density is expected with the addition of WO_3 content due to the replacement of the lighter weight Ge ions with the heavier W ions.

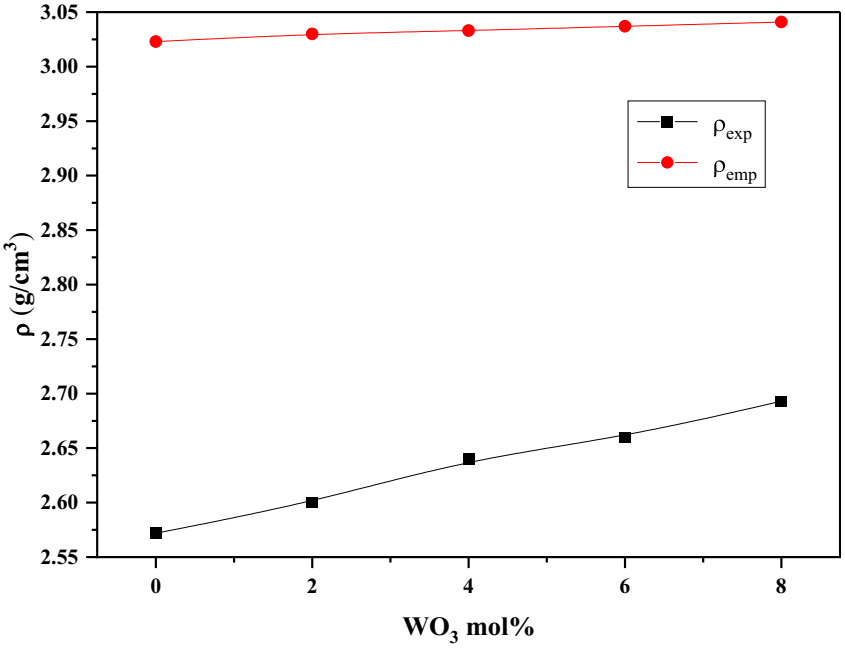

Fig. 1. The change in density as function of WO_3 content.

Molar volume is closely connected to the internal spatial structure of materials, so, it is appropriate to provide the molar volume values of the examined glasses as well [16]. The computed values of the molar volumes for both empirical and experimental calculations are shown in Fig. 2. As the WO_3 content increases, the molar volume of empirical calculation exhibits a linear behaviour, while the experimental measurements show a progressive drop. Molar volume may be reduced because of the formation of the shorter atomic links, which may have increased the stretching force constant of the glass network bonds [15].

The oxygen packing density (O P D) values can be obtained by the following equation [17],

$$O.P.D = \frac{\rho.O}{M_i} \tag{1}$$

where, O is the number of oxygens per unit Formula.

The obtained values of O.P.D, given in Table (1), show a decreasing trend with the gradual addition of WO_3.

The values of the average boron–boron separation distance $\langle d_{B\text{-}B} \rangle$ were also obtained by using equation (2),

$$d_{B-B} = \left[\frac{V_m^b}{N_A}\right]^{\frac{1}{3}} \tag{2}$$

where N_A is Avogadro's number and V_m^b is the volume of boron per mole of the sample, which it can be calculated using equation (3),

$$V_m^b = \frac{V_m}{2(1-\chi_B)} \tag{3}$$

where X_B is the mole fraction of boron [16].

The W^{3+} ion concentration in all samples was also calculated using equation (4),

$$N_W = n\left[\frac{wt_{WO_3}}{Mw_{WO_3}}\right]\rho N_A \tag{4}$$

where Wt_{WO_3} is the percentage weight in the glass sample and Mw_{WO_3} is the molecular weight of WO_3.

The Polaron radius (r_p) can be calculated from equation (5),

$$r_p = \frac{1}{2}\left(\frac{\pi}{6N}\right)^{\frac{1}{3}} \tag{5}$$

where N is the number of W^{3+} ion concentration in the sample [18].

The inter-nuclear distance is given by,

$$r_i = \left(\frac{1}{N}\right)^{\frac{1}{3}} \tag{6}$$

while the field strength (F) can be calculated as follows,

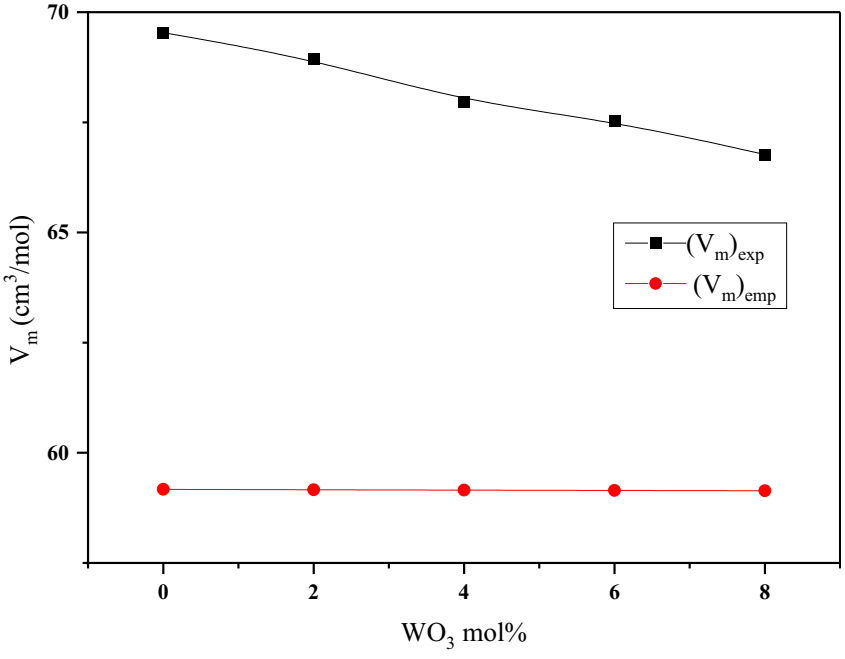

Fig. 2. The change in molar volume as a function of WO_3 content.

Table 1. The obtained values of the measured and calculated physical parameters of the glasses under study.

Physical parameter for the glass samples.	S1	S2	S3	S4	S5
ρ_{exp} g/cm^3	2.57	2.60	2.64	2.66	2.69
ρ_{emp} g/cm^3	3.02	3.03	3.03	3.04	3.04
$(V_m)_{emp}$ cm^3/mole	59.17	59.16	59.15	59.15	59.14
$(V_m)_{exp}$ cm^3/mole	69.54	68.94	67.97	67.53	66.77
$d_{B\text{-}B}$ (10^{-8} m)	4.77	4.75	4.73	4.72	4.70
N. of W (10^{20} cm^{-1})	–	1.26	1.27	1.28	1.30
r_p (10^{-7} m)	–	2.00	1.99	1.98	1.98
r_i (10^{-8} m)	–	8.05	8.01	7.99	7.96
F (10^{16} cm^{-2})	–	1.14	1.15	1.16	1.17
OPD × 10^{22} (Atom/cm^3)	8.66	8.73	8.86	8.91	9.02

$$F = \frac{Z}{r_p^2} \tag{7}$$

where z in the atomic number.

Table 1 shows the field strength and polaron radius of the glasses under investigation. It is noted the field strength increases with the increase of WO_3 ratio. This increase is due to the increase in interatomic distance and to the increase in the number of NBO ions because of the convert of BO_4 to BO_3.

3.2. FTIR spectra

Figure 3 displays the IR absorption spectra for glass samples spanning the 400 to 2000 cm^{-1} wavenumber range. The sample S_1 deconvoluted FTIR spectrum, seen in Fig. 4, was produced by analysing the band of functional groups attached to glass using a deconvolution technique. The deconvolution peaks are related to the active peaks inside the glass network. The peaks can be coordinated as following: The combined bending vibration of Si–O–Si in [SiO_4] causes a peak of about 480 cm^{-1} [19–21]. The band at 588-554 cm^{-1}, which coincides with the vibrations of W–O bonds, relates to the O–Si–O mode. The Na^+ vibration within the glass network is what causes the band to form at 529 cm^{-1}

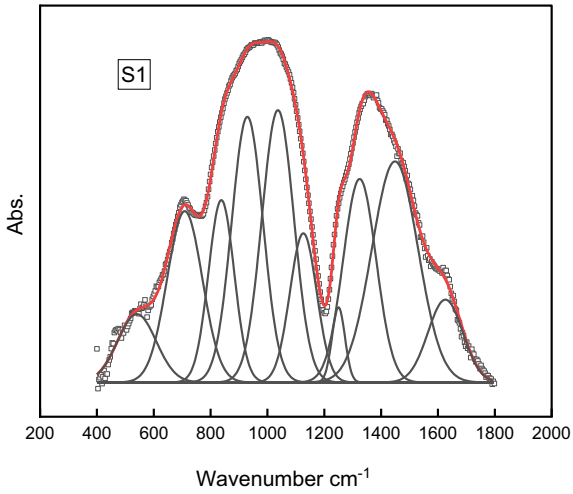

Fig. 4. Deconvoluted FTIR spectrum for S1 sample.

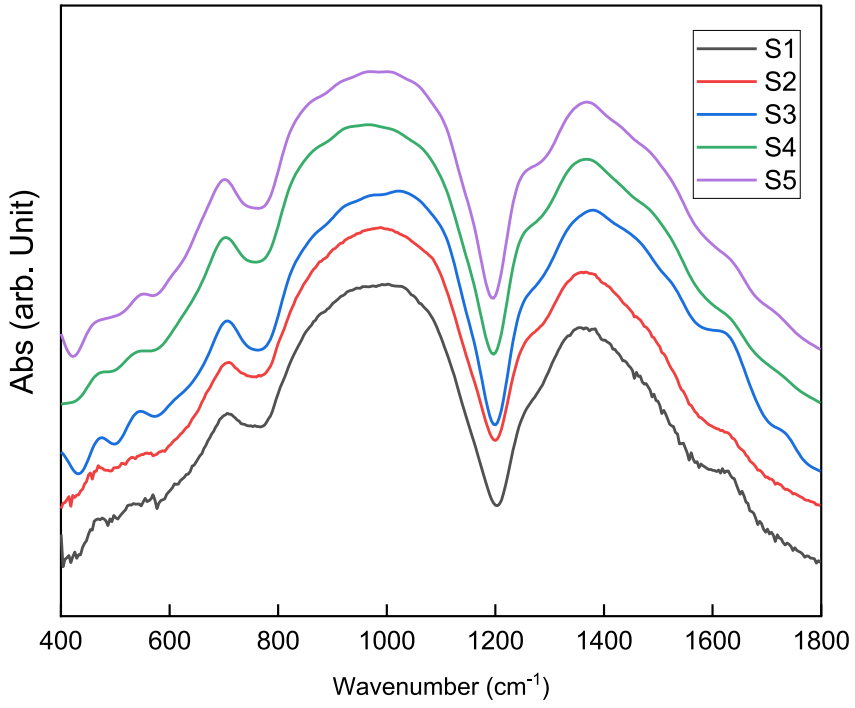

Fig. 3. The FTIR spectra of the glass samples.

Table 2. FTIR absorption spectra analysis of the prepared glass samples.

	S1	S2	S3	S4	S5
Centre	490.00	480.49	474.00	479.07	469.77
Area	2.52	0.84	1.36	1.34	0.39
Centre	–	568.49	590.00	545.77	555.90
Area	–	2.01	2.32	2.57	2.72
Centre	685.00	704.43	707.43	710.00	720.00
Area	9.50	9.25	10.14	11.25	11.91
Centre	845.00	847.66	853.66	854.02	863.50
Area	16.61	13.33	10.51	9.20	8.90
Centre	950.00	950.37	958.37	960.00	965.00
Area	18.32	14.73	12.25	11.96	10.41
Centre	1020.00	1044.04	1051.04	1090.46	1020.43
Area	10.59	10.87	9.98	9.72	9.33
Centre	1133.00	1123.02	1128.02	1120.00	1114.35
Area	10.01	10.08	10.76	10.98	11.76
Centre	1280.00	1273.46	1262.46	1260.00	1258.00
Area	7.71	10.06	13.49	15.45	16.59
Centre	1463.00	1487.04	1481.04	1480.00	1477.00
Area	11.02	11.31	13.69	13.70	14.08
Centre	1683.00	1680.00	1666.00	1630.00	1627.13
Area	8.85	7.23	6.18	5.03	2.03
N_4	0.48	0.42	0.34	0.32	0.29

[22]. The peak vibrations around 670 cm^{-1} and 720 cm^{-1} are related to B–O–B vibrations, which come from di-borate B_4O_7 (670 cm^{-1}) and penta-borate B_5O_8 (720 cm^{-1}) [23,24].

The band at 860 cm^{-1} could be attributed to the stretching vibrations B–O in tetrahedral BO_4 in penta-borate groups [25,26]. The peak at 920 cm^{-1} represents the Si–O^- stretching vibration of [SiO_4] tetrahedron, the Si–O–B stretching vibration and the B–O^- stretching vibration mode of [BO_4] tetrahedron [27,28]. The band at 1020 to 1088 cm^{-1} refers to the B–O stretching vibrations of BO_4 in tri-borate groups [29]. Overlapping of the asymmetric stretching vibration of Si–O in the [SiO_4] tetrahedron, and the reduction in peak strength means a reduction in the bridging oxygen [30,31]. 1182 cm^{-1} band referred to the B– O stretching vibrations of BO_3 orthoborate groups [32,33]. 1261 cm^{-1} band attributed to the stretching vibrations of B– O^- in BO_3 [34]. The band located at ~1420 and 1490 cm^{-1} may be due to B–O stretching vibration in BO units [35]. The band at 1640 cm^{-1} is O–H vibration [29,33]. $N_4 = A_4/(A_3 + A_4)$ was used to calculate the amount of quadruple boron, N_4. A_4 and A_3 represent the relative areas of the BO_4 and BO_3, respectively. Deconvoluted FTIR spectra are shown Fig. 4 and in details in Table 2. The behaviour of N4 within the addition of WO_3 is shown in Fig. 5.

3.3. Optical measurements results

The band gap of optical energy (E_{opt}), the refractive index (n), and the Urbach energy (E_u) The optical parameters of the glass system, such as the optical band gap energy (E_{opt}), Urbach energy (E_U), and refractive index (n), are determined with the use of UV–Vis spectrophotometer measurements. Using the Beer–Lambert law [36], the following features may be utilized to describe the structure of the glass host at any given light incident:

$$I_t = I_0 e^{-\alpha t} \tag{8}$$

(t) is the sample's thickness, (I_t) and (I_0) denote the light's incidence and transmittion intensities, respectively. I_0 is the total amount of light.

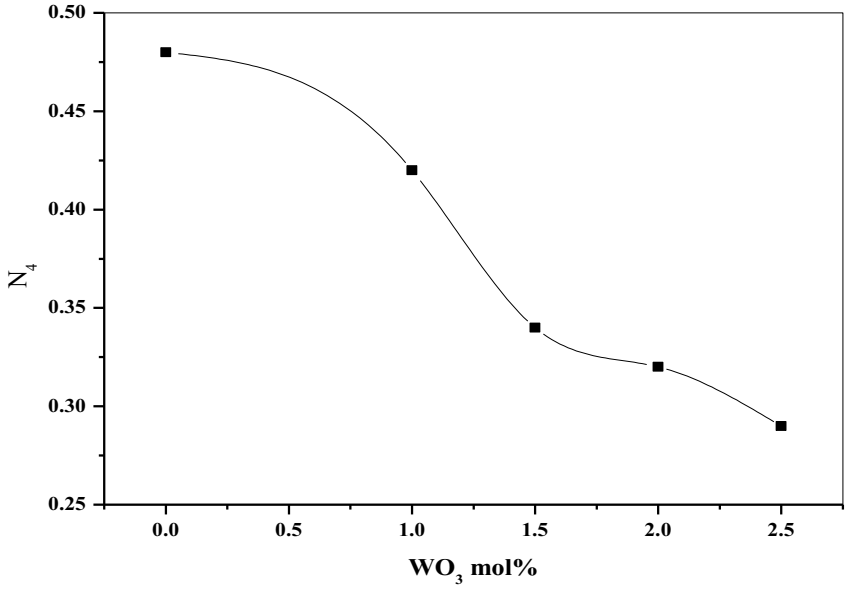

Fig. 5. Dependence of N_4 on the WO_3 content.

The optical absorption spectra obtained using UV–Vis spectroscopy are shown in Fig.(6) it is confirmed the amorphous nature of the prepared glass samples since they showed clear absorption edges. The transmission spectra of glass samples are also shown in Fig. (7). Due to nearly the same shape of the spectra with increasing WO_3 concentration, this reveals that all the prepared glass samples have interesting optical properties [37].

Meanwhile, the Davis and Mott relation [38] can be used to find the optical band gap energy (E_{opt}) of the glass samples:

$$\alpha h\nu = B\left(h\nu - E_{opt}\right)^{n} \quad (9)$$

where h ν is incident photon energy, B is a constant, E_{opt} is the optical band gap energy, and α is the absorption coefficient. With n = 2 or 1/2 for permitted indirect and direct transition, the value of n refers to E_{opt}.

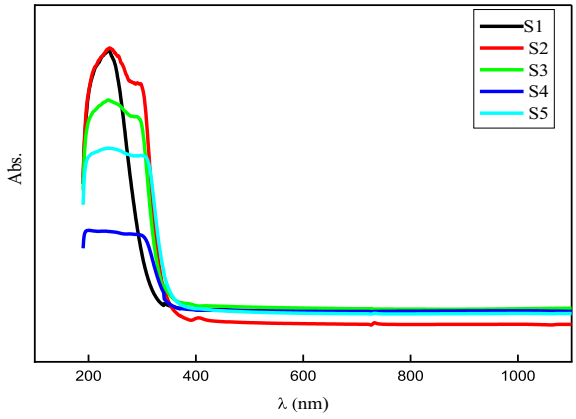

Fig. 6. The optical absorbance spectra for all the glass samples.

Urbach energy (E_U) is the length of the absorption edge's exponential tail which is determined by the following empirical relation [39],

$$\alpha = \alpha_0 e^{\frac{h\nu}{E_U}} \quad (10)$$

where E_U is the width of the band tails of localised states, v is the radiation frequency, and α_0 is a constant.

The values of the indirect optical band gap energy were calculated using the relationship between $(\alpha h\nu)^{0.5}$ and (hν) Fig. (8) [38–41]. On the other hand, as shown in Fig. (9), The calculation of the Urbach energy values [39,41,42] was made using the relation between ln (α) and (hν). As seen in Fig. (10), structural variations of the glasses under study caused the energy gap and Urbach energy data to be vary dramatically. In the considered borate network, the generation of non-bridging oxygens increased the disorder state.

The refractive index (n), of any substance is an important physical property. It basically has control over the material's optical and electrical characteristics. Additionally, it is directly related to the domestic fields present in the substance and the ions and the electronic polarizability (p). The study of the connection between (n) and (p) for any semiconducting material is of consider a scientific interest because it has some of optoelectronic

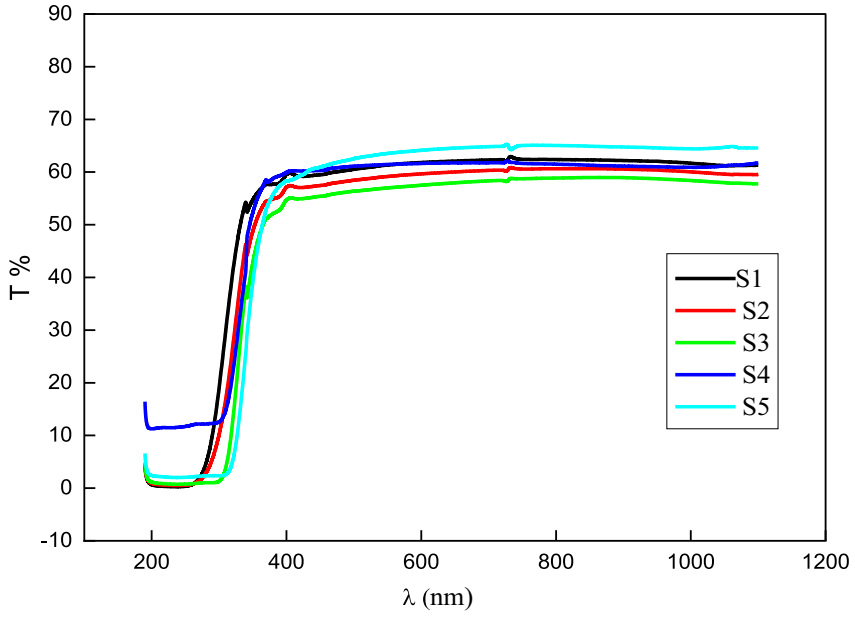

Fig. 7. The optical transmittance spectra for all the glass samples.

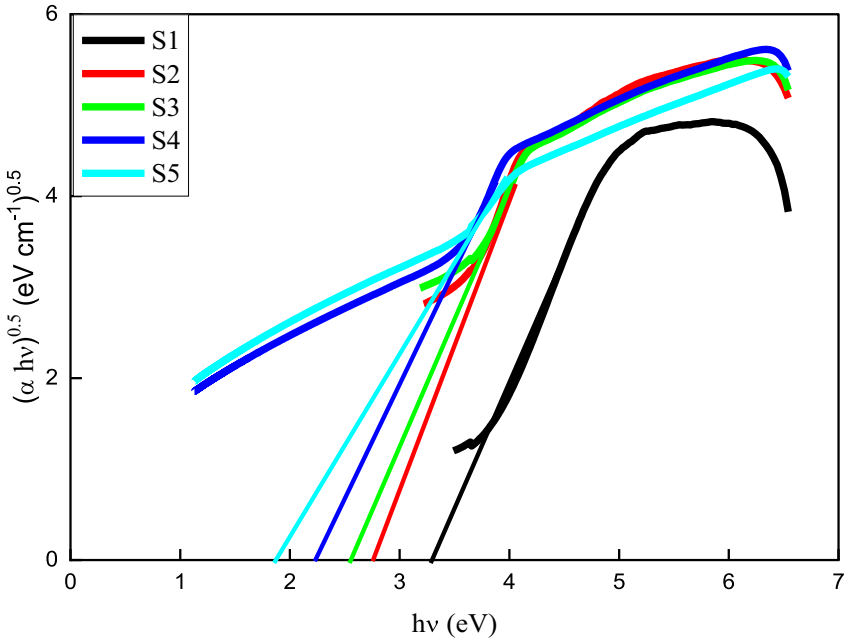

Fig. 8. The change of $(\alpha h\nu)^{0.5}$ with hν for the prepared glass samples.

applications and devices [42]. The higher polarizability of W^{3+} cations in glass system that caused the increase of (n) [43].

The refractive index (n) calculated using the following formula using the optical band gap energy (E_{opt}) [44],

$$\frac{n^2-1}{n^2+2}=1-\sqrt{\frac{E_{opt}}{20}} \quad (11)$$

Molar refraction (R_m) is the result of reflection loss ($(n^2-1)/(n^2+2)$) and molar volume (V_m). This parameter is produced by the Lorentz–Lorentz equation, where R_m is proportional to V_m, and it has the following implications for the glass structure [45],

$$R_m=\left(\frac{n^2-1}{n^2+2}\right)V_m \quad (12)$$

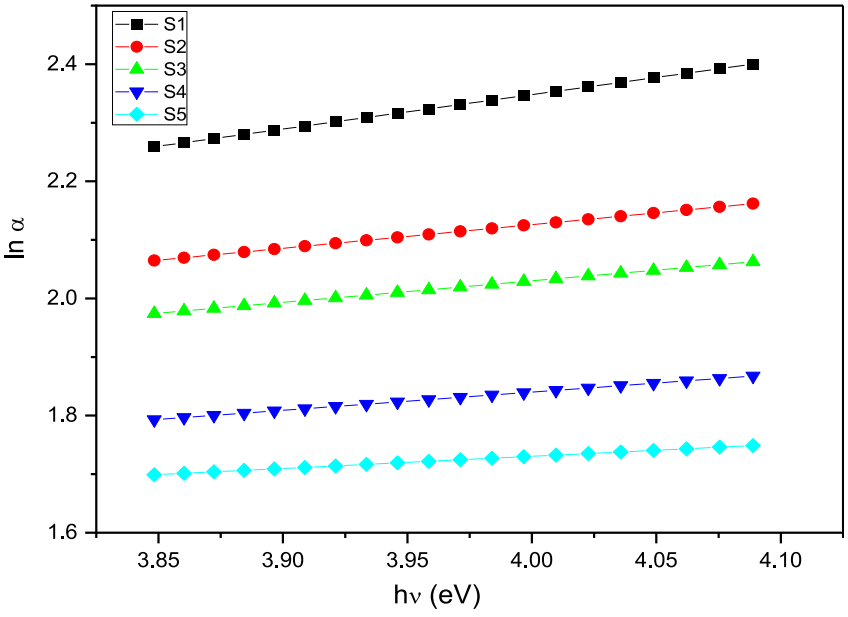

Fig. 9. The variation of ln (α) with hν of the prepared glass samples.

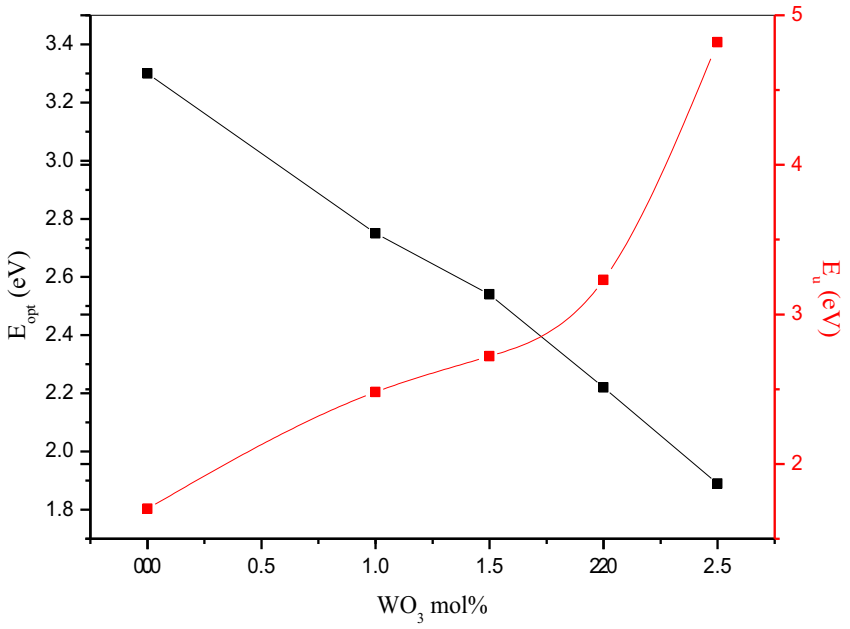

Fig. 10. The relation of E_{opt} and E_u with WO_3 content.

The molar electronic polarizability αm, according to Clausios Mosotti, is given by the relation:

$$\alpha_m = \left(\frac{3}{4\pi N_A}\right) R_m \tag{13}$$

where N_A is Avogadro's number.

Optical basicity (Λ) and electronic polarizability (α_0^{2-}) values can be obtained of Eg by using the formulas as: [46,47].

$$\alpha_0^{2-} = -0.24192 E_{opt} + 3.5 \tag{14}$$

$$\Lambda = -0.1344 E_{opt} + 1.7 \tag{15}$$

As the W^{3+} concentration was increased, the electronic polarizability of oxide and the optical basicity increase (Table 3). This indicates that the oxygen ions in the present glass system have the chance to transfer electrons to the surrounding cations [47].

Table 3. Optical parameters in the glasses sample.

Optical parameter	S1	S2	S3	S4	S5
E_{opt} (eV)	3.30	2.75	2.54	2.22	1.89
E_U (eV)	1.70	2.48	2.72	3.23	4.82
Refractive index, n	1.98	2.10	2.15	2.24	2.35
optical electronegativity (χ)	0.89	0.74	0.68	0.60	0.51
Metallization	0.51	0.47	0.45	0.43	0.40
dielectric constant	3.92	4.41	4.62	5.01	5.52
electronic polarizability (α_0^{2-})	2.70	2.83	2.89	2.96	3.04
optical basicity (Λ)	1.26	1.33	1.36	1.40	1.45

The optical electronegativity (χ) can be calculated based on E_{opt} by applying this relation [47]:

$$\chi = 0.2688 E_{opt} \tag{16}$$

The kind of bonding existing in the materials is also indicated by optical electronegativity (χ). The values χ are found to decrease when WO_3 levels increases in the network glasses. This decrease is brought on by its inverse relationship to the refractive index. The modest changes in electronegativity values might perhaps be caused by the system's covalent nature [48,49].

Metallization criterion (M) gives the non-metallic or metallic nature of the oxide glasses, where Rm/Vm > 1 for metal and <1 for non-metal [49]. Higher values of M are the trend of material or compound that has larger optical band gap (E_{opt}) and smaller refractive index (n) and vice versa [50,51]. Insulating material has M near 1. A relation can be derived from the Lorentz–Lorenz equation,

$$M = 1 - \frac{R_m}{V_m} \tag{17}$$

where V_m is the molar volume of the respective glass sample. The M data showed almost linear decrease as WO_3 increased, these results are shown in Table 3. However, the increment in WO_3 concentration in the glass system caused decrease in M values due to the contraction of E_{opt} [47].

Optical dielectric constant, ε_{opt} can be calculated using the equation:

$$\epsilon_{opt} = n^2 \quad (18)$$

According to Table 3, the ε_{opt} showed increasing trend with the WO_3 increasing from 3.91 to 6.50. The increase may be due to the rise in NBO in the network of glass samples due to the addition of WO_3.

4. Conclusion

From this work we can conclude that the FTIR result showed that BO_3 increased and BO_4 decreased with increasing WO_3 content, accordingly, NBO increases. The density measurements confirmed the glassy state of the prepared samples. The optical band gap, optical electronegativity and Metallization showed decreased values while Urbach energy, Optical band gap show high value, 3.3 eV for x = 0 which decreases to 1.89 eV for sample 8 mol % with increase in refractive index from 1.98 up to 2.35 the refractive index, dielectric constant, electronic polarizability and optical basicity increased with increasing WO_3 content. These results let us conclude that these samples are promising in electrical, energy storage and opto-electronic applications.

Conflicts of interest

The authors have no conflict of interest to declare related to the content of the article.

References

[1] Dantas NO, Ayta WEF, Silva ACA, Cano NF, Silva SW, Morais PC. Effect of Fe_2O_3 concentration on the structure of the SiO_2-Na_2O-Al_2O_3-B_2O_3 glass system. Spectrochim Acta Mol Biomol Spectrosc 2011 Oct 15;81(1):140–3.

[2] Aboutaleb D, Douglad J, Safi B, Jbara O, Iratni A. Phase separation and chemical durability in the SiO_2 -B_2O_3 -Na_2O (SBN) glass system. Asian J Chem 2012;24(2):473–80.

[3] Zheng H, Zhen-Ou J, Strano MS, Kaner RB, Mitchell A, Kalantar ZK. Nanostructured tungsten oxide-properties, synthesis, and applications. Adv Funct Mater 2011;21: 2175–96.

[4] Lee WJ, Fang YK, Ho JG, Hsieh WT, Ting SF, Huang D, et al. Effects of surface porosity on tungsten trioxide (WO_3) films' electrochromic performance. J Electron Mater 2000;29:183–7.

[5] Kreidl NJ. Recent applications of glass science. J Non-Cryst Solids 1990;3(1):377–84. 123.

[6] Singh AK, Singh D, Thind KS, Mudahar GS. Barium-borate-flyash glasses: as radiation shielding Materials. Nucl Instrum Methods Phys Res, Sect B 2008;266(1):140–6.

[7] Mhareb MA, Almessiere MA, Sayyed MI, Alajerami YM. Physical, structural, optical and photons attenuation attributes of lithium magnesium-borate glasses: role of Tm_2O_3 doping. Optik 2019;182:821–31.

[8] Lakshminarayana G, Kumar A, Dong MG, Sayyed MI, Long NV, Mahdi MA. Exploration of gamma radiation shielding features for titanate bismuth borotellurite glasses using relevant software program and Monte Carlo simulation code. J Non-Cryst Solids 2018;481:65–73.

[9] Singh N, Singh R, Singh KJ, Sing K. γ-Ray shielding properties of lead and bismuth borosilicate glasses. Glass Technol 2005;46(4):311–4.

[10] Glumglomchit P, Rajagukguk J, Kaewkhao J, Kirdsiri K. A novel radiation shielding material for gamma-ray: the development of lutetium lithium borate glasses. Key Eng Mater 2018;766:246–51.

[11] Kaur P, Singh KJ, Thakur S. Evaluation of the gamma radiation shielding parameters of bismuth modified quaternary glass system. AIP Conf Proc 2018;1953(1):090031.

[12] Alajerami YS, Drabold D, Mhareb M, Cimatu KA, Chen G, Kurudirek M. Radiation shielding properties of bismuth borate glasses doped with different concentrations of cadmium oxides. Ceram Int 2020;46(8):12718–26.

[13] Pascuta P, Pop L, Rada S, Bosca M, Culea E. The local structure of bismuth germanate glasses and glass ceramics doped with europium ions evidenced by FT-IR spectroscopy. Vib Spectrosc 2008;48(2):281–4.

[14] Zhou B, Lin H, Chen B, Yue-Bun PE. Super broadband near-infrared emission in Tm-Bi codoped sodium-germanium-gallate glasses. Opt Express 2011;19(7):6514–23.

[15] Mundher M, Bendary AA, Farag MA, El-Bediwi Abu Bakr, Hassaan MY. Tungsten oxide effects on conductivity, dielectric parameters, and density of sodium germanium borosilicate glass. J Mater Sci Mater Electron 2023;34:1069.

[16] Abu-raia WA, Farag MA, El-Khateeb SA, Aly Saeed. Impact of Gd3+ on optical, local structure, and attenuation properties of lead borosilicate glasses. Egypt J Chem 2023;66(No. 9): 125–32.

[17] Berkemeier F, Voss S, Imre AW, Mehrer H. Molar volume, glass-transition temperature, and ionic conductivity of Na- and Rb-borate glasses in comparison with mixed Na–Rb borate glasses. J Non-Cryst Solids 2005;351:3816.

[18] Reddy RR, Nazeer Y, Abdul Azeem P, Rama GK, Rao TR, Buddhudu S, et al. Absorption and emission spectral studies of Sm^{3+} and Dy^{3+} doped alkali fluoroborate glasses. J Quant Spectrosc Radiat Transfer 2003;77:149.

[19] Morsi RM, Basha MA, Morsi MM. Synthesis and physical characterization of amorphous silicates in the system SiO_2-Na_2O– RO (R=Zn, Pb or Cd). J Non-Cryst Solids 2016;439: 57–66.

[20] Silva AM, Queiroz CM, Agathopoulos S, Correia RN, Fernandes MH, Oliveira JM. Structure of SiO_2–MgO–Na_2O glasses by FTIR, Raman and ^{29}Si MAS NMR. J Mol Struct 2011;986:16–21.

[21] Ervino CZ, Michel AA. Raman and infrared investigations of glass and glass-ceramics with composition $2Na_2O \cdot 1CaO \cdot 3SiO_2$. J Mater Res 1994;9(1):216–25.

[22] Alomairy S, Al-Buriahi MS, Abdel Wahab EA, Sriwunkum C, Shaaban K, Synthesis. FTIR, and neutron/charged particle transmission properties of Pb_3O_4–SiO_2–ZnO–WO_3 glass system. Ceram Int 2021;47:17322–30.

[23] Hivrekar MM, Sablea DB, Solunke MB, Jadhav KM. Network structure analysis of modifier CdO doped sodium borate glass using FTIR and Raman spectroscopy. J Non-Cryst Solids 2017;474:58–65.

[24] Kumar D, Rao SM, Singh SP. Structural, optical and thermoluminescence study of Dy^{3+} ion doped sodium strontium borate glass. J Non-Cryst Solids 2017;464:51–5.

[25] Gomaa HM, Moneep AM, Bendary AA, Yahia IS, Zahran HY. Structural and optical absorption coefficient analysis of barium lead sodium-borate glass doped with graphene nano-powder. Optik 2022;271:170090.

[26] Susheela KL, Madhu A, Eraiah B, Kokila MK. Effect of certain alkaline metals on Pr doped glasses to investigate spectroscopic studies. IOP Conf Ser Mater Sci Eng 2018;310: 012052.

[27] Othman HA, Elkholy HS, Hager IZ. FTIR of binary lead borate glass. Struct Invest 2016;1106:286–90.

[28] Aboalatta A, Asad J, Humaid M, Musleh H, Shaat SK, Ramadan K, et al. Experimental investigation of zinc sodium borate glass systems containing barium oxide for gamma

radiation shielding applications. Nucl Eng Technol 2021;53: 3058−67.
[29] Prabhu NS, Somashekarappa HM, Sayyed MI, Osman H, Alamri S, Khandaker MU, et al. Structural and optical modifications in the BaO-ZnO-LiF-B_2O_3-Yb_2O_3 glass system after g-Irradiation. Materials 2021;14:6955.
[30] Hassaan MY, Saudi HA, El-Bahnasawy HH, Bendary AA, Abdel-Moety AS. Preparation and characterization of Egyptian granite based glass with different Na^+ ions content. Silicon 2022;14:4485−91.
[31] Abdelgawad KM, Ahmed GM, Farag AM, Bendary AA, Tartor BA, Bashter II, et al. Eco-friendly transparent glass prepared from rice straw ash for neutron and charged particle radiation shielding. Ann Nucl Energy 2023;191:109939.
[32] Farouk M, Samir A, Ibrahim A, Farag MA, Solieman A. Raman, FTIR studies and optical absorption of zinc borate glasses containing WO_3. Appl Phys A 2020;126:696.
[33] Mansour E. FTIR spectra of pseudo-binary sodium borate glasses containing TeO_2. J Mol Struct 2012;1014:1−6.
[34] Ahmed K, Gomaa HM, Bendary AA, Mohammad SS, Saudi HA. Structural and radiation shielding parameters of heavy metal-based environment-friendly glass systems for nuclear radiation security applications. J Phys Chem Solid 2023;181:111526.
[35] Bhargavi K, Sudarsan V, Brik MG, Sundara RM, Gandhi Y, Nageswara RP, et al. Influence of Al declustering on the photoluminescent properties of Pr^{3+} ions in PbO−SiO_2 glasses. J Non-Cryst Solids 2013;362:201−6.
[36] El-Mallawany R. Tellurite glasses part 1. Elastic properties. Mater Chem Phys 1998;53:93−120.
[37] Kaewjaeng S, Chanthima N, Thongdang J, Reungsri S, Kothan S, Kaewkhao J. Synthesis and radiation properties of Li_2O-BaO-Bi_2O_3-P_2O_5 glasses, Mater. Today Proc 2021;43:2544−53.
[38] Mott NF, Davis EA. Electronic processes in non-crystalline materials. Oxford University Press; 2012.
[39] Tuyen VP, Sengthong B, Quang VX, Van DP, Van TH, Xuan HL. Dy^{3+} ions as optical probes for studying structure of boro-tellurite glasses. J Lumin 2016;178:27−33.
[40] Saddeek YB, Afifi H, Abd El-Aal N. Interpretation of mechanical properties and structure of TeO_2-Li_2O-B_2O_3 glasses. Phys B Condens Matter 2007;398:1−7.
[41] Lopez R, Gome RZ. Band-gap energy estimation from diffuse reflectance measurements on sol-gel and commercial TiO_2: a comparative study. J Sol Gel Sci Technol 2011;61:1−7.
[42] Sabri NS, Yahya A, Talari MK. Anomalous optical properties of xSrO−10PbO− (90−x) B_2O_3 glass system. Trans Indian Inst Met 2017;70:557−65.
[43] Halimah MK, Ami Hazlin MN, Muhammad FD. Experimental and theoretical approach on the optical properties of zinc borotellurite glass doped with dysprosium oxide. Spectrochim Acta Mol Biomol Spectrosc 2018;195:128−35.
[44] Hasanuzzaman M, Rafferty A, Sajjia M, Olabi AG. Properties of glass materials. 2016.
[45] Halimah MK, Faznny MF, Azlan MN, Sidek HA. Optical basicity and electronic polarizability of zinc borotellurite glass doped La^{3+} ions. Results Phys 2017;7:581−9.
[46] Dimitrov V, Sakka S. Electronic oxide polarizability and optical basicity of simple oxides. J Appl Phys 1996;79: 1736−40.
[47] Pavani PG, Sadhana K, Mouli VC. Optical, physical and structural studies of boro-zinc tellurite glasses. Phys B Condens Matter 2011;406:1242−7.
[48] Azlan M, Halimah M, Shafinas S, Daud W. Polarizability and optical basicity of Er^{3+} ions doped tellurite-based glasses. Chalcogenide Lett 2014;11:319.
[49] Chimalawong P, Kaewkhao J, Kedkaew C, Limsuwan P. Optical and electronic polarizability investigation of Nd^{3+} doped soda-lime silicate glasses. J Phys Chem Solid 2010;71: 965−70.
[50] Dimitrov V, Komatsu T. Classification of oxide glasses: a polarizability approach. J Solid State Chem 2005;178: 831−46.
[51] Dimitrov V, Komatsu T. An interpretation of optical properties of oxides and oxide glasses in terms of the electronic ion polarizability and average single bond strength (Review). J Univ Chem Technol Metall 2010;45:219−50.